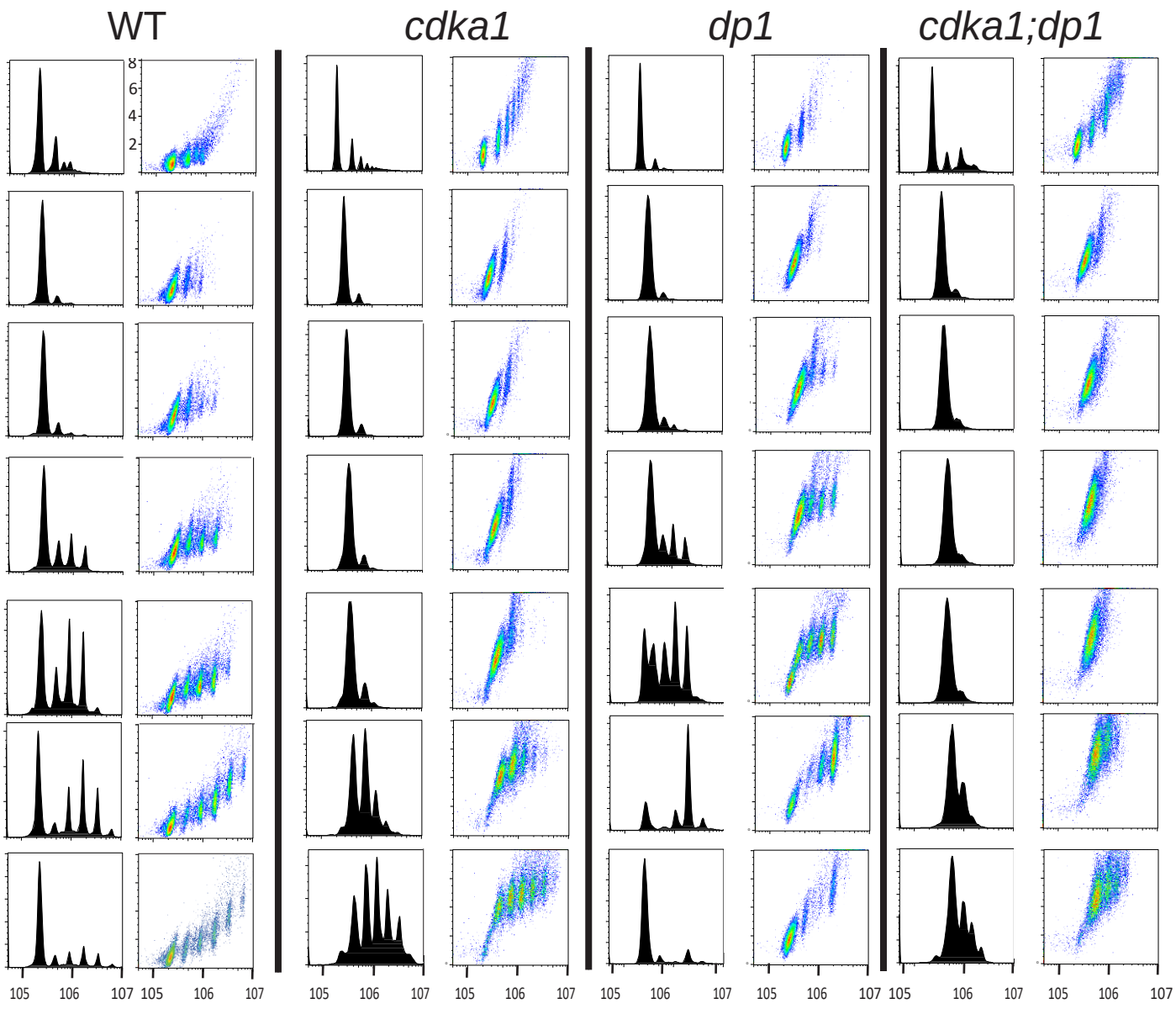
WT
cdka1
dp1
cdka1;dp1
8
6
4
2
105
106
107

Figure S1. Flow cytometric analysis of WT and *cdka1* cell cycles, and interaction of *cdka1* and *dp1*. Related to Figure 1. The indicated strains were synchronized by nitrogen deprivation/refeeding, and analyzed by flow cytometry. Hours after release indicated on left. Histograms: DNA (Sytox; log scale). Scatterplots: DNA (log scale, x) vs. forward scatter (FSC, linear scale; units * 10^-6, y). All plots of Sytox or FSC have the same axis values as indicated by hatch marks. Bottom: subpopulations from the 12 hr WT sample: 1,2,4,8: large cells after 0,1,2,3 rounds of synchronous DNA replication; N: newly hatched, with low FSC (small size) and slightly lower DNA signal than the large 1C cells due to large-cell background. Note that divisions are highly synchronous and multiple- fission daughters stay in the mother cell wall until hatching, so DNA peaks at 1,2,…2^n are observed. See STAR Methods for discussion of *Chlamydomonas* FACS analysis.

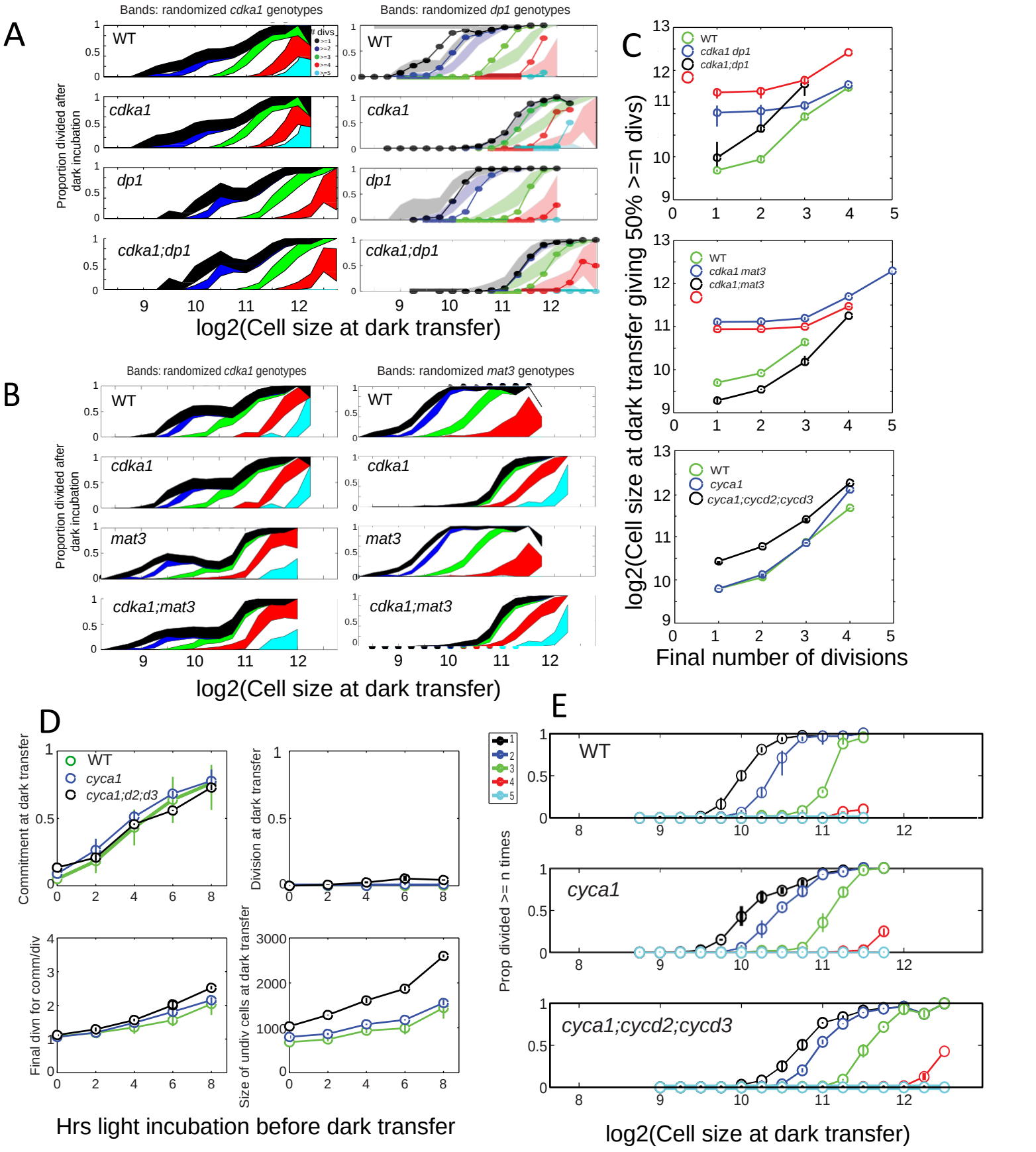
A
Bands: randomized cdka1 genotypes
Bands: randomized dp1 genotypes
WT
cdka1
dp1
cdka1;dp1
divs
Proportion divided after dark incubation
log2(Cell size at dark transfer)
B
Bands: randomized cdka1 genotypes
Bands: randomized mat3 genotypes
WT
cdka1
mat3
cdka1;mat3
Proportion divided after dark incubation
log2(Cell size at dark transfer)
C
WT
cdka1 dp1
cdka1;dp1
cdka1 mat3
cdka1;mat3
cyca1
cyca1;cycd2;cycd3
log2(Cell size at dark transfer giving 50% >=n divs)
Final number of divisions
D
WT
cyca1
cyca1;d2;d3
Commitment at dark transfer
Division at dark transfer
Final divn for comm/div
Size of undiv cells at dark transfer
Hrs light incubation before dark transfer
E
WT
cyca1
cyca1;cycd2;cycd3
Prop divided >= n times
log2(Cell size at dark transfer)

Figure S2. Effects of *cdka1* and *dp1*, of *cdka1* and *mat3*, and of *cycA1, cycD2* and *cycD3* on commitment. A. Monte Carlo evaluation of statistical significance of effects of *cdka1* genotype in WT and *dp1* backgrounds. Related to Figure 4.

See STAR Methods for description of the procedure. The colored bands contain 99% of simulated datasets constructed by selection from the real data without replacement, without regard to *cdka1* genotype. The line graphs indicate the actual data from the experiment (see Figure 4). (The dataset used for this simulation was a subset of the final one graphed in Figure 4; this does not affect the conclusions). The graphs can be read as follows: the WT curves for all division numbers, and especially the smaller division numbers, is clearly outside of the 99% band to the left (smaller cells for a given division number). The *cdka1* curves for lower division numbers are outside the bands to the right; the curves for larger division numbers are inside the bands. Therefore, *cdka1* disruption increases the cell size threshold for small division numbers but not large ones. The graphs for *dp1* and *cdka1;dp1* provide the same conclusion for the *dp1* background. **B**. As in **A**, but from an experiment with two each *WT, cdka1, mat3*, *cdka1;mat3* strains. Pooled raw data for the two strains is in the line graphs; bands as in **A. C:** From the curves for cumulative division number vs. log2(Cell size at dark transfer) in Figures 4,S2B,E, the size at which the curve hit 50% was determined by interpolation for each number of divisions, and plotted. The graph shows that *cdka1* disruption blocks divisions at smaller cell sizes but gives a cell size-to-division number like *CDKA1* for larger cell sizes (top two graphs; blue and red curves start flat (1,2,3 divisions), joining corresponding green and black *CDKA1* curves at ~3 divisions). *dp1* and *mat3* disruption shift critical sizes for all division numbers uniformly to larger and smaller size respectively. *cyca1* disruption has little effect, but combined with *cycd2-1;cycd3-1* mutations has a similar effect to *dp1* disruption. It is untested whether subsets of this triple cyclin mutant would have the same effect. In these graphs, the error bars (perpendicular bars) represent the range of values for two strains of each genotype tested in parallel in each experiment. Most of these 'error bars' are so small as to be confined within the marker contour. Due to a requirement for a minimal amount of data to support a plotted point, some points only derive from one sample (no error bar) and some division numbers lack sufficient data to be plotted (no point). **D,E:** WT, *cyca1::PARO*, and *cyca1::PARO;cycd2-1;cycd3-1* triple mutants (2 strains each) were tested as in Figures 2,4. *cyca1::PARO* has little discernable effect on kinetics of commitment either with respect to time or cell size; the triple mutant shifts commitment to all division numbers to larger cell size, but has no effect on commitment timing.

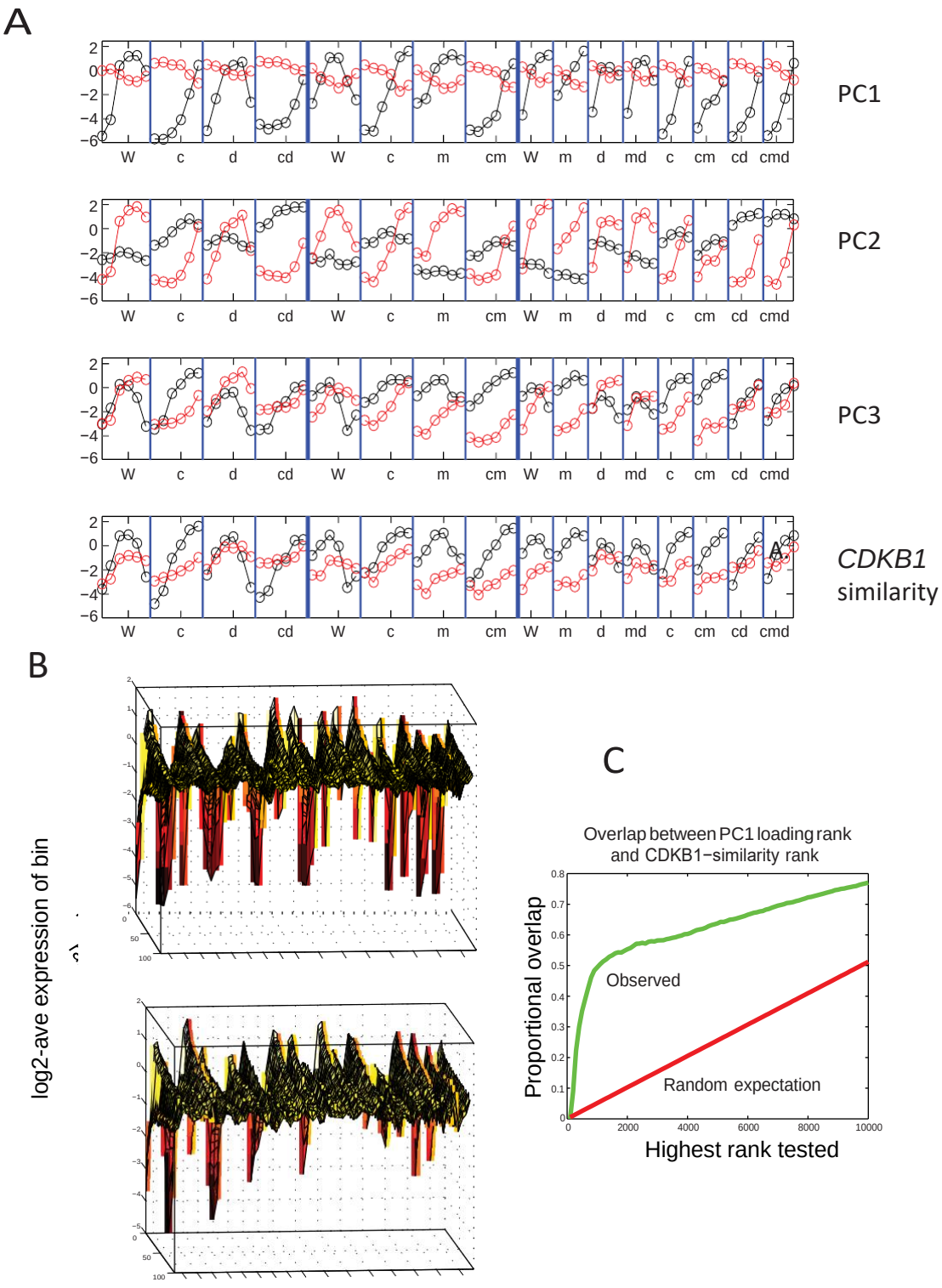
A
PC1
PC2
PC3
CDKB1
similarity
W c d cd W c m cm W m d md c cm cd cmd
B
log2-ave expression of bin
C
Overlap between PC1 loading rank
and CDKB1−similarity rank
Proportional overlap
Observed
Random expectation
Highest rank tested

Figure S3. The mitotic regulon accounts for most variability in gene expression across the experiments. A. Related to Figure 6. Expression levels of the genes with the top (black) and bottom (red) 100 loadings for PC1,2,3, and the top and bottom 100 genes in Euclidean distance from *CDKB1* (representative of the mitotic regulon) are graphed by experiment (experiment abbreviations. Note similarity of the patterns of top-loaded PC1 and PC3, bottom-loaded PC2, and top CDKB1-similar genes. **B.** Top: log2 of expression of the first 10,000 genes in PC1-loading order were averaged in bins of 100 and plotted sequentially to make a surface. The highly regulated pattern of expression through the experiments (plotted in the same order as in **A**) of the most PC1-similar genes ramifies (with decreasing amplitude) through a large proportion of the transcriptome (19,526 transcripts). Bottom: the same analysis based on Euclidean distance from *CDKB1*, with a similar pattern. **C.** Sorting by PC1 loading and *CDKB1*-similarity causes high overlap in gene lists. The graph plots the proportion of overlap between the two lists, going to increasingly high ranks (so, for example, the top-2000 lists overlap >50%). The random expectation is shown in red.

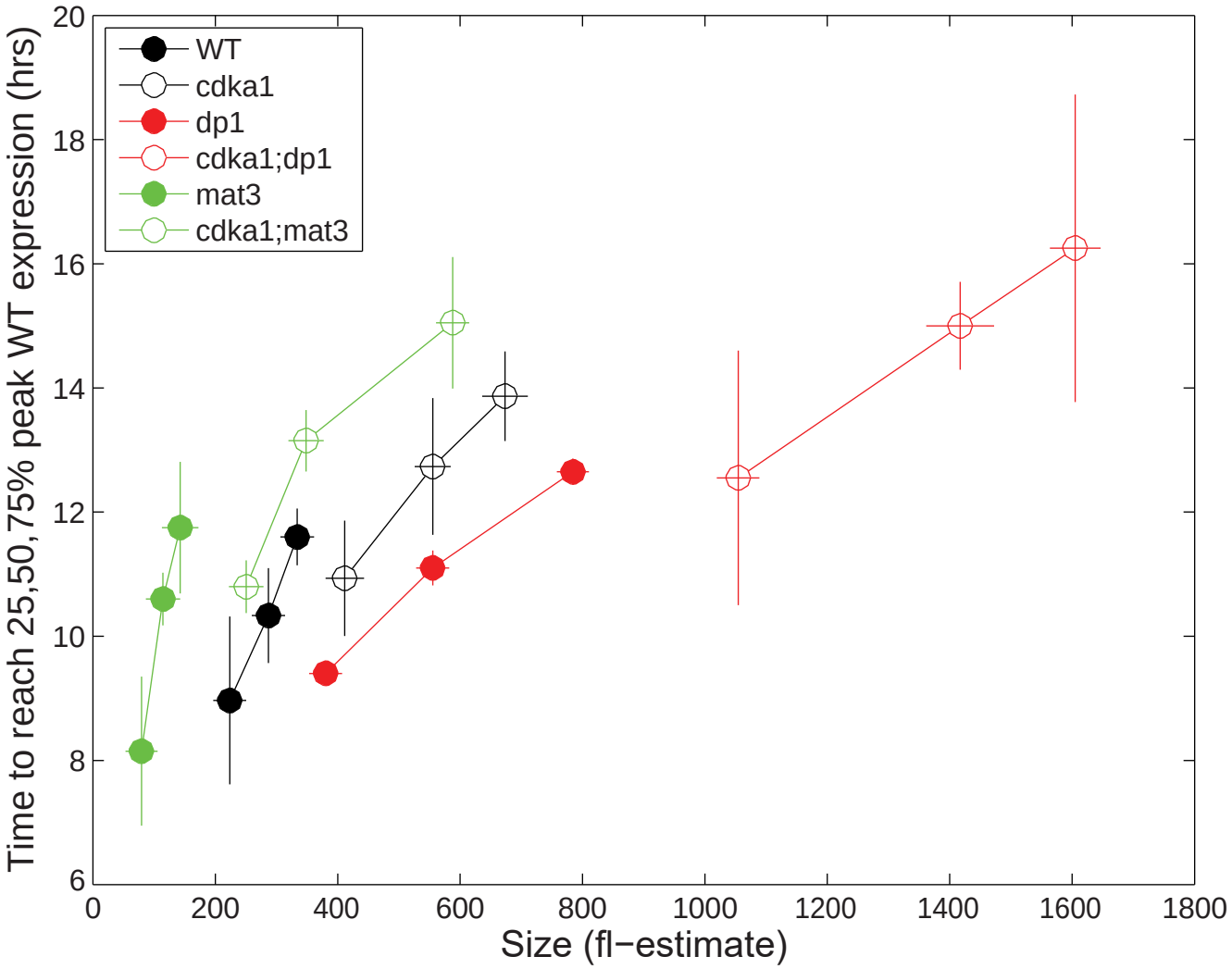
WT
cdka1
dp1
cdka1;dp1
mat3
cdka1;mat3
Time to reach 25,50,75% peak WT expression (hrs)
Size (fl−estimate)
20
18
16
14
12
10
8
6
0
200
400
600
800
1000
1200
1400
1600
1800

Figure S4. Time and cell size of induction of the mitotic regulon. Related to Figure 7. From the data in Figure 6C, times when expression reached 25%, 50% and 75% of WT peak was determined by interpolation. The cell sizes at these times for each genotype were determined by interpolation from the graphs in Figure 5. The data come from two experiments for each curve; the range of values in x and y are shown by the error bars. The cell sizes are in femtoliter (fl) estimates from FACS FSC values (Figures 1, S1, 5; data not shown), using an empirically determined approximation fl=26 + 48.6 * (FSC * 10^-6)^2. This approximation was determined by measurement of Coulter channelyzer femtoliter modes of a set of live-cell samples, compared to FACS FSC values for the same samples fixed for flow cytometry, varying from FSC ~1.5 to ~30 *10^6 and from
~75 to ~1600 fl (data not shown).

	Starting	2C	newly hatched	Size ratio	# divisions to achieve hatched size
WT	1.6 +/- 0.1 (3)	3.8 +/- 0.3 (3)	1.2 +/- 0.2 (3)	10.0	3.3
cdka1	1.7 +/- 0.2 (3)	6.0 +/- 0.2 (3)	1.4 +/- 0 (2)	18.4	4.2
dp1	2.0 +/- 0 (2)	5.2 +/- 0.1 (2)	2.3 +/- 0.2 (2)	5.1	2.4
cdka1; dp1	2.6 +/- 0.4 (2)	7.7 +/- 0.5 (2)	NA	8.8	3.1
mat3	0.8 +/- 0.1 (2)	2.3 +/- 0 (2)	1.0 +/- 0 (2)	5.3	2.4
cdka1; mat3	1.4 +/- 0 (2)	5.2 +/- 0.2 (2)	1.1 (1)	22.4	4.5
mat3; dp1	1.8 (1)	4.3 (1)	2.0 (1)	4.6	2.2
cdka1; mat3; dp1	3.0 (1)	7.7 (1)	NA	6.6	2.7

Table S1. Analysis of cell size in FACS profiles. Related to Figures 1, 5. From the three synchronization experiments (Figures 1, S1; data not shown for experiment 3), forward scatter (FSC) values for three populations were determined. Estimation was from the full numerical output file from the FACS scanner, which was processed by custom MATLAB software that provided the mode (after 5-point data smoothing) of the selected populations. The table presents modal values, mean +/- standard deviation; number of replicates in parentheses. Starting population: the 1C cells in cultures blocked by nitrogen deprivation. 2C: cells in the replicative period that completed their first DNA replication cycle (approximate center of the distribution; Figure 1 bottom: 'Division size'). Newly hatched: first detectable new daughters from completion of replication, division and hatching (Figure 1 bottom: 'Hatching size'). Size ratio: FSC values are approximately proportional to the square root of electronic live cell volume based on an empirical test with a set of samples with a wide range of sizes (data not shown). Therefore, the ratio of cell volumes between 2C and newly hatched is estimated as (FSC_2C/FSC_hatched)^2 ('Size ratio'). For *cdka1;dp1* and *cdka1;mat3;dp1* there was insufficient recovery of hatched cells by the end of the timecourse for a reliable estimate so the starting population was used for the size ratio as an alternative estimate of new daughter size. '# divisions to achieved hatched size' is just the log2 of the size ratio. NA –not available; insufficient hatching by the end of the time course to provide a reliable number.

	Initial cell sizes: mean +/- sd (n)	Fold WT	P vs WT (t-test)
WT	616 +/-16 (9)		
cdka1	793 +/- 164 (6)	1.29	0.010
mat3	440 +/- 0 (2)	0.71	0.004
dp1	760 +/- 57 (2)	1.23	0.013
cdka1;mat3	700 +/- 141 (2)	1.14	0.180
cdka1;dp1	1230 +/- 156 (2)	2.00	$\ll$0.0001
cyca1	790 +/- 99 (2)	1.28	0.008
cyca1;cycd2;cycd3	880 +/- 0 (2)	1.43	0.0002

Table S2. Sizes of initial light-starved daughter cells in commitment experiments. Related to Figures 2, 4. Cells were cultured in photoautotrophic medium in the dark to allow completion of all ongoing and committed division cycles, then plated on photoautotrophic medium for the commitment assay. For each experiment, the mean cell size in pixels at time of plating (determined with automatic segmentation; Figure 1, bottom) was determined. The mean and standard deviation of those mean values across 'n' experiments (indicated) is presented in the table, as well as the fold WT and P-value vs. WT by 2-sample t-test. (Note that this size measurement is based on pixel number following automated image segmentation of a brightfield image; thus the scaling relationship of the units to cell volume is unknown, though clearly higher values imply bigger cells.)

	TAP preculture	Gametes
WT	80 +/- 17	59 +/- 7
cdka1	125 +/- 18	76 +/- 15
mat3	43 +/- 8	16 +/- 1
cdka1;mat3	87 +/- 9	52 +/- 1

Table S3. Cell sizes after gametogenesis. Related to Figures 1, 5. Strains of the indicated genotypes (from three tetratype tetrads from a cross of *mat3::PARO* to *cdka1::HYGRO*; thus three of each genotype) were grown on TAP agar to a dense patch. Cells were resuspended in gamete-induction medium M-N/5, and electronic volumes recorded (entries are mean +/- standard deviation of approximate modal value from a Coulter Counter Channelyzer). The cultures were then incubated in the light overnight to induce gamete formation, and electronic volumes recorded again. This cross was at the 4th backcross of *mat3-5* into the congenic background in which *cdka1::HYG* was isolated. *mat3* mutant cultures can accumulate suppressors of their small size phenotype [S1]; this experiment demonstrates a uniform small size phenotype of *mat3* strains used in the present experiments, therefore absence of suppressors. The size phenotype of *mat3* in these experiments and this strain background is much stronger in gametogenesis than in proliferating daughter cells, for unknown reasons.

Strain	Genotype	Figures
1264-1D	WT	Figures 5,6 (expt 1)
1264-1C	*cdka1::HYGRO*	Figures 5,6 (expt 1)
P10	WT	Figure 2, S2D,E
M10	WT	Figures 2, 6, S1 (expt 3)
1205-1A	*cdka1::HYGRO*	Figure 2
1205-2A	*cdka1::HYGRO*	Figure 2
1335-3	WT	Figure 3
1335-4	WT	Figure 3
1335-19	cdka1::HYGRO	Figure 3
1335-20	cdka1::HYGRO	Figure 3
1264-1D	WT	Figure 4
1264-3D	WT	Figure 4
1264-1C	*cdka1::HYGRO*	Figure 4
1264-3A	*cdka1::HYGRO*	Figure 4
1264-1A	*dp1::PARO*	Figure 4
1264-3C	*dp1::PARO*	Figure 4
1264-1C	*cdka1::HYGRO;dp1::PARO*	Figure 4
1264-3A	*cdka1::HYGRO;dp1::PARO*	Figure 4
1252-3C	WT	Figure S2B
1252-4B	WT	Figure S2B
1252-3B	*cdka1::HYGRO*	Figure S2B
1252-4A	*cdka1::HYGRO*	Figure S2B
1252-3D	*mat3::PARO*	Figure S2B
1252-4D	*mat3::PARO*	Figure S2B
1252-3A	*cdka1::HYGRO;mat3::PARO*	Figure S2B
1252-4C	*cdka1::HYGRO;mat3::PARO*	Figure S2B
1264-1A	*dp1::PARO*	Figs S1,5,6 (expt 1)
1264-1B	*cdka1::HYGRO;dp1::PARO*	Figs 5,6 (expt 1)
1266-1B	WT	Figs S1,1,5,6 (expt 2)
1266-1A	*cdka1::HYGRO*	Figs 5,6 (expt 2)
1266-1D	*mat3::PARO*	Figs 5,6 (expt 2)
1266-1C	*cdka1::HYGRO;mat3::PARO*	Figure 6 (expt 3)
1285-4D	*mat3::PARO*	Fig 6 (expt 3)
1284-5B	*dp1::PARO*	Figure 6 (expt 3)
1286-6D	*mat3::PARO;dp1::PARO*	Figure 6 (expt 3)
1282-1A	*cdka1::HYGRO*	Figure 6 (expt 3)
1285-3B	*cdka1::HYGRO;mat3::PARO*	Figure 6 (expt 3)
1284-3C	*cdka1::HYGRO;dp1::PARO*	Figure 6 (expt 3)
1286-6A	*cdka1::HYGRO;mat3::PARO;dp1 ::PARO*	Figure 6 (expt 3)
1040-3D	*cyca1::PARO*	Figure S2D,E
K166-4D	*cyca1::PARO*	Figure S2D,E
1039-6B	*cyca1::PARO;cycd2;cycd3*	Figure S2D,E
1039-6C	*cyca1::PARO;cycd2;cycd3*	Figure S2D,E

Table S4. **Strains used. Related to STAR Methods.** In all commitment experiments, two strains of each genotype were tested, in a near-uniform genetic background (CC4402/CC4403 background), named here P10 and M10. In –N/synchrony and RNAseq experiments, one strain of each genotype was tested; confirmation was from an independent experiment (*mat3;dp1* and *cdka1;mat3;dp1* genotypes were tested only in one experiment; see text). *dp1::PARO* and *mat3::PARO*) (provided by J. Umen) were backcrossed to 4402/4403 at least 5 times before use except for x1229 and x1230 segregants, 2X-backcrossed. *cycA1::PARO* was crossed into this background previously [S2]. The *cycd2-1* and *cycd3- 1* mutations were isolated in the CC402/4403 background as adventitious passenger mutations in a screen for ts-lethal cell cycle mutations [S3]. *cycd3-1* is a premature stop codon at position 19 (chromosome_6:5448827 CA E19*, also chromosome_6:5448879 CA M1I removing start codon, both in Cre06.284350); *cycd2-1* (chromosome_6:6082068 CT) mutates the essential splice donor dinucleotide /GT to /AT, potentially truncating the expressed protein at codon 139 in the middle of the cyclin homology region. The efficacy of these mutations in ablating CYCD2 or CYCD3 protein expression has not been directly established.

Supplemental References

S1. Fang, S.-C., and Umen, J.G. (2008). A suppressor screen in chlamydomonas identifies novel components of the retinoblastoma tumor suppressor pathway. Genetics *178*, 1295–1310.

S2. Atkins, K.C., and Cross, F.R. (2018). Interregulation of CDKA/CDK1 and the Plant-Specific Cyclin-Dependent Kinase CDKB in Control of the Chlamydomonas Cell Cycle. Plant Cell *30*, 429–446.

S3. Breker, M., Lieberman, K., and Cross, F.R. (2018). Comprehensive Discovery of Cell-Cycle-Essential Pathways in Chlamydomonas reinhardtii. Plant Cell *30*, 1178–1198.

S4. Merchant, S.S., Prochnik, S.E., Vallon, O., Harris, E.H., Karpowicz, S.J., Witman, G.B., Terry, A., Salamov, A., Fritz-Laylin, L.K., Maréchal-Drouard, L., *et al.* (2007). The Chlamydomonas genome reveals the evolution of key animal and plant functions. Science *318*, 245–250.

S5. Blaby, I.K., Blaby-Haas, C.E., Tourasse, N., Hom, E.F.Y., Lopez, D., Aksoy, M., Grossman, A., Umen, J., Dutcher, S., Porter, M., *et al.* (2014). The Chlamydomonas genome project: a decade on. Trends Plant Sci. *19*, 672–680.

S6. Langmead, B., and Salzberg, S.L. (2012). Fast gapped-read alignment with Bowtie 2. Nat. Methods *9*, 357–359.